Contents lists available at ScienceDirect

Ceramics International

Highly spectrum-selective near-band-edge ultraviolet photodiode based on indium oxide with dipole-forbidden bandgap transition

Yanan Huang [a], Yongfeng Li [a,b,*], Rui Deng [c], Bin Yao [a,b,*], Zhanhui Ding [a], Ligong Zhang [d], Haifeng Zhao [d], Zhenzhong Zhang [d], Lei Liu [d], Yingrui Sui [e]

[a] State Key Lab of Superhard Material, College of Physics, Jilin University, Changchun 130012, PR China
[b] Key Laboratory of Physics and Technology for Advanced Batteries (Ministry of Education), College of Physics, Jilin University, Changchun 130012, PR China
[c] School of Materials Science and Engineering, Changchun University of Science and Technology, Changchun 130022, PR China
[d] State Key Lab of Excited State Processes, Changchun Institute of Optics, Fine Mechanics and Physics, Chinese Academy of Sciences, Changchun 130033, PR China
[e] Key Laboratory of Functional Materials Physics and Chemistry of the Ministry of Education, Jilin Normal University, Siping 136000, Jilin, PR China

ARTICLE INFO

ABSTRACT

We reported a highly spectrum-selective ultraviolet photodiode based on In_2O_3 with dipole-forbidden bandgap transition. The near-band-edge ultraviolet emission and absorption were observed in the hybrid In_2O_3 films with the In_2O_3 nanocrystals embedded into the amorphous In_2O_3 matrix, indicating that the dipole-forbidden rule of bulk In_2O_3 is broken. The hybrid In_2O_3 film was deposited on the p-GaN/sapphire wafer to form an In_2O_3/p-GaN heterojunction photodiode. The photodiode showed an obvious rectifying behavior in a current–voltage measurement and a narrow-band ultraviolet photoresponse at the near-band-edge region under back-illumination conditions. Electronic structure calculations based on the first-principles method demonstrate that the breaking of dipole-forbidden transition rule is derived from the surface states of In_2O_3 nanocrystals. Our results suggest that tailoring the In_2O_3 nanocrystalline structure is an effective route to achieving novel optical properties and applying these properties to the ultraviolet optoelectronic field.

© 2016 Elsevier Ltd and Techna Group S.r.l. All rights reserved.

1. Introduction

Wide-bandgap oxides have attracted much attention due to their excellent properties and functionalities [1–13]. Among these oxides, indium oxide (In_2O_3) is extensively applied in the fields of solar cells, liquid crystal displays and photovoltaic devices, due to its outstanding properties of combining high transparency in the visible-spectrum range with high electrical conductivity [14–21]. Owing to the dipole-forbidden nature of the band-edge quantum states of In_2O_3, there exists an energy difference between the fundamental bandgap of ~ 2.9 eV and the optical bandgap of ~ 3.8 eV [22–24]. The symmetry properties of the conduction-band minimum (CBM) and valence-band maximum (VBM) states of the In_2O_3 prohibit the near-band-edge (NBE) transition, involving the process of light emission and absorption. Therefore, it is commonly believed that In_2O_3 is not a suitable light emitter and absorber in the NBE region (near the fundamental bandgap energy), which hinders its potential application in the ultraviolet

(UV) optoelectronic field, such as photodiodes (PDs) and light-emitting diodes (LEDs). Nevertheless, recent research suggests that the dipole-forbidden rule can be broken and the strong NBE UV emission was observed in the nanostructural In_2O_3 [25–28]. Therefore, In_2O_3 nanoengineering is a suitable route to break dipole-forbidden rule and realize UV emission/absorption at the NBE region, which can be used to fabricate high-efficiency UV light emitting and detecting devices.

In this paper, we fabricated the hybrid In_2O_3 films with the In_2O_3 nanocrystals embedded into the amorphous matrix. Photoluminescence (PL) and optical absorption properties of the hybrid In_2O_3 films were investigated in detail. The hybrid In_2O_3 film was deposited on p-GaN to form a heterojunction photodiode. A narrow-band UV photoresponse at the NBE region under back-illumination conditions was observed. The physical mechanism of the breaking of dipole-forbidden rule in the In_2O_3 nanocrystals is also discussed in detail through first-principles calculations.

2. Experimental and first-principles calculations details

The In_2O_3 thin films were deposited on the quartz substrates at room temperature using pure argon (Ar) as the working gas by

---

* Corresponding authors at: State Key Lab of Superhard Material, College of Physics, Jilin University, Changchun 130012, PR China.
E-mail addresses: liyongfeng@jlu.edu.cn (Y. Li), binyao@jlu.edu.cn (B. Yao).

radio frequency (rf) magnetron sputtering method. Commercial available high-purity In_2O_3 target (purity > 99.99%) with stoichiometric proportion was used in our experiments. The vacuum chamber was evacuated to a base pressure of 10^{-4} Pa before the film deposition and the sputtering pressure was controlled to 0.1 Pa. In order to wipe off impurities on the surface of the In_2O_3 target, the target was pre-sputtered by Ar gas for 10 min before the In_2O_3 layer was deposited on the substrate. The growth process of the In_2O_3 layer lasted for one hour. The as-grown In_2O_3 film was annealed at 400 °C in air for 30 min in a horizontal quartz tube furnace. For the preparation of In_2O_3-based heterojunction photodiode, the In_2O_3 layer was first deposited on the commercial available p-type GaN/sapphire wafer at room temperature and then was annealed at 400 °C in air. The Ni/Au electrodes were deposited through a shadow mask on the p-type GaN layer and served as the p-type electrode. The indium metal was sintered on the In_2O_3 layer and served as the n-type electrode.

The crystal structure characterizations were performed by using X-ray diffraction (XRD) with Cu Kα radiation of 1.5406 Å. The surface morphologies and compositions were characterized and recorded using a field-emission scanning electron microscope (FESEM) with an energy dispersive X-ray spectrum (EDS) analyzer. A high-resolution transmission electron microscope (HRTEM) was used to examine the crystalline structure of the hybrid In_2O_3 thin films. The optical absorption spectra were recorded using an UV–vis–near-IR spectrophotometer. The PL measurements were performed using a He–Cd laser with a 325 nm line as the excitation source. The current–voltage curves were measured at room temperature in order to further verify the formation of the p–n heterojunction. The spectral response of the In_2O_3-based heterojunction photodiode was recorded using the 150 W Xe lamp, monochromator, chopper and lock-in amplifier. The illumination light is shed onto the heterojunction from the p-GaN side.

First-principles calculations of the electronic structures were carried out using the density functional theory (DFT) as implemented in the Vienna ab-initio simulation package (VASP) code with the projector augmented wave (PAW) potentials [29,30]. The generalized gradient approximation (GGA) to the exchange-correlation functional was used. The cutoff energy for the plane-wave basis set is 500 eV. For the indium atoms, d states were treated as valence states. For the bulk In_2O_3, a 40-atom supercell with bixbyite structure was used in the calculations on the band structures and optical properties. To integrate over the Brillouin zone (BZ), a $2 \times 2 \times 2$ k-point mesh was used. An In_2O_3 quantum dot (QD) with a diameter of 1.5 nm, including 55 indium and 84 oxygen atoms, is cut from the bixbyite bulk In_2O_3.

3. Results and discussion

Fig. 1a shows the typical XRD patterns of as-grown and 400 °C annealed In_2O_3 films deposited on quartz substrates. No diffraction peak is observed for the as-grown In_2O_3 film, indicating an amorphous structure. For the 400 °C annealed In_2O_3 film, there exist weak diffraction peaks and the matching of observed 2θ values with the standard In_2O_3 diffraction data confirms that the annealed film is crystallized with a cubic structure. To further check the crystal structure after being annealed, we performed the TEM measurement. The TEM image of the In_2O_3 film after being annealed is shown in Fig. 1b. It can be seen that the In_2O_3 nanocrystals are embedded in the amorphous matrix, indicating a hybrid In_2O_3 nanocrystals/amorphous film. The nanocrystal size is estimated to be several nanometers. The surface and cross-sectional SEM images of the annealed In_2O_3 thin film are shown in Fig. 1c and d, respectively. It is observed that the film is compact with a thickness of ~1.2 μm. In addition, we also examined the proportion of indium and oxygen elements using EDS analyzer. The indium and oxygen compositions are 41.28 at% and 58.72 at% for the as-grown film, as well as 41.12 at% and 58.88 at% for the annealed film, respectively, suggesting that the stoichiometric proportions of indium and oxygen elements of the films are slightly larger than 2:3.
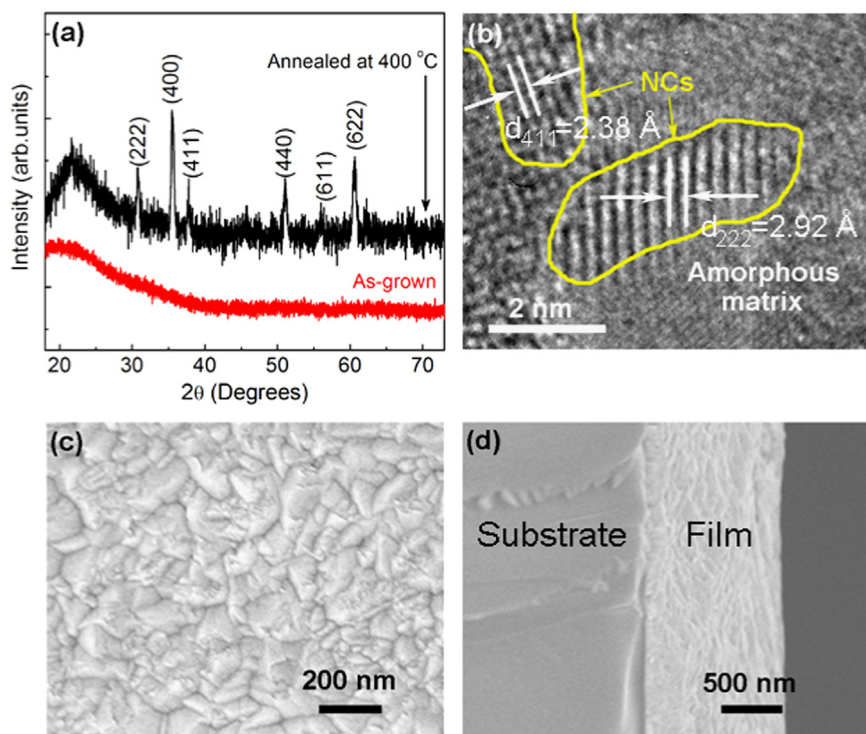

Fig. 1. (a) XRD patterns of the as-grown and 400 °C annealed In_2O_3 thin films grown on quartz substrates. (b) TEM image, (c) surface and (d) cross-sectional SEM images of the annealed In_2O_3 thin film.
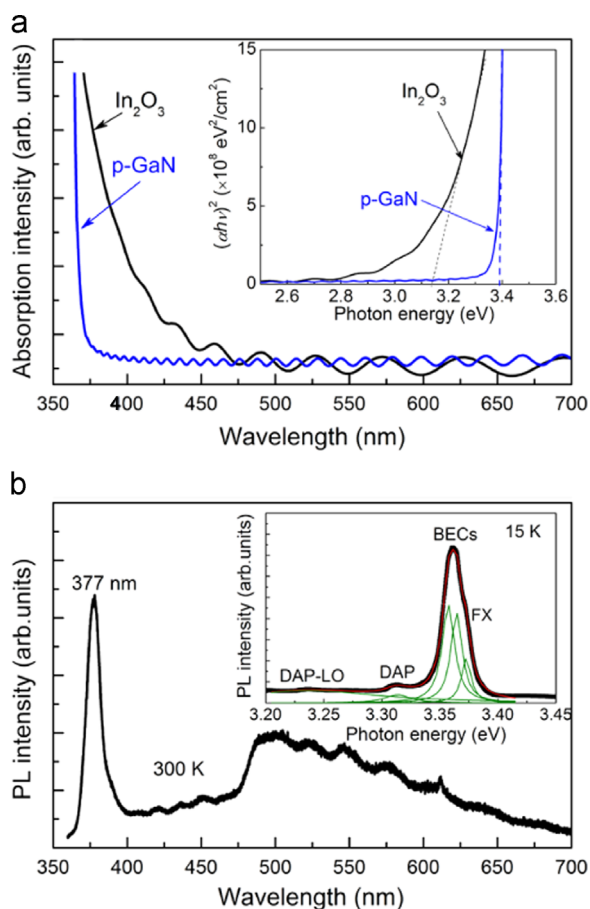
Fig. 2. (a) Optical absorption spectrum of the 400 °C annealed In$_2$O$_3$ thin film grown on quartz substrate. The inset in (a) shows the determination of the corresponding optical bandgap. The optical absorption spectrum of the p-type GaN wafer used for fabricating the photodiode is also shown in (a). (b) Room temperature PL spectrum of the 400 °C annealed In$_2$O$_3$ thin film grown on quartz substrate. The inset in (b) shows the corresponding 15 K PL spectrum.

Fig. 3. (a) Schematic illustration of In$_2$O$_3$/p-GaN heterojunction photodiode. (b) Current–voltage curve of the In$_2$O$_3$/p-GaN heterojunction. The inset in (b) shows the I–V characteristic between two indium contacts on the In$_2$O$_3$ film. (c) Spectral response of the In$_2$O$_3$/p-GaN heterojunction under various biasing. The inset in (c) shows the time-dependent photocurrent at the bias of −5 V when a 380 nm light irradiates on the device with periodical turning on and off.

To determine the optical properties of the annealed In$_2$O$_3$ film, we performed the optical absorption spectrum measurement, as shown in Fig. 2a. A strong band tail absorption in the range of 370–450 nm is observed for the annealed In$_2$O$_3$ film. According to the relationship between absorption coefficient α and photon energy $h\nu$, the optical bandgap is determined to be 3.14 eV, as shown in the inset of Fig. 2a, which is close to the fundamental bandgap of bulk In$_2$O$_3$ (2.9 eV) [2] and much lower than the widely quoted optical bandgap of 3.75 eV [31]. This result indicates that the dipole-forbidden rule of bulk In$_2$O$_3$ is broken in the annealed In$_2$O$_3$ film with the nanocrystals embedded in the amorphous matrix. The optical absorption spectrum of the p-GaN substrate is also shown in Fig. 2a for afterwards clarifying the origin of the spectral response in the In$_2$O$_3$/p-GaN heterojunction. The optical bandgap of the p-GaN is determined to be 3.4 eV, which is consistent with the previous reports [32,33].

We also checked the room temperature PL spectra of the annealed In$_2$O$_3$ film, as shown in Fig. 2b. A strong and sharp UV emission peak at 377 nm (3.289 eV) is observed, indicating that the dipole-forbidden rule of bulk In$_2$O$_3$ is broken [2,34]. This result is consistent with the optical absorption spectra. A weak visible emission band is also observed, which is caused by indium interstitial [35]. To investigate the origin of the UV peak, we performed the low temperature PL measurement. The inset in Fig. 2b shows the corresponding 15 K PL spectrum in the UV region, which is similar with the results reported by Wei et al. [25]. There exist five peaks at 3.371, 3.362, 3.357, 3.317 and 3.237 eV by fitting the PL
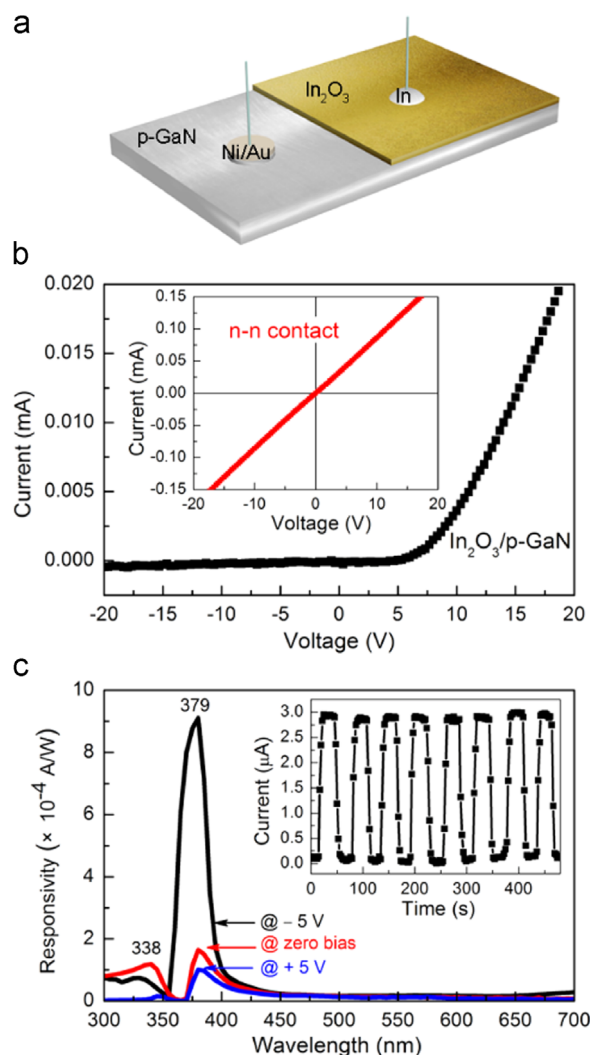
data with five sub-peaks. The peaks at 3.371, 3.317 and 3.237 eV are derived from the radiative recombination of free-exciton (FX), donor–acceptor pair (DAP) and its first-order longitudinal optical (LO)-phonon replica, respectively [36]. There has been no clarity on the origin of the two peaks at 3.362 and 3.357 eV, but Wei et al. tentatively assigned them to the radiative recombination of bound-exciton-complex (BEC) [25].

To explore the possibility of applying NBE optical properties of In$_2$O$_3$ film in the optoelectronics field, we deposited the In$_2$O$_3$ film on the p-GaN substrate at room temperature and followed an annealing process at 400 °C to form the In$_2$O$_3$/p-GaN heterojunction. The In$_2$O$_3$-based photodiode is fabricated from the heterojunction and its structure is shown in Fig. 3a. Fig. 3b shows the current–voltage (I–V) characteristics of the photodiode in darkness at room temperature. The In$_2$O$_3$/p-GaN heterojunction shows an obvious rectifying behavior, indicating the formation of a p–n junction diode. The turn-on voltage is 6.2 V for the heterojunction. It is known that series resistance (R_s) and ideality factor (n) are very important parameters to characterize performance of diode, which can be calculated using the equation $dV/d(\ln I) = nkT/q + IR_s$. The obtained values of the series resistance and the ideality factor
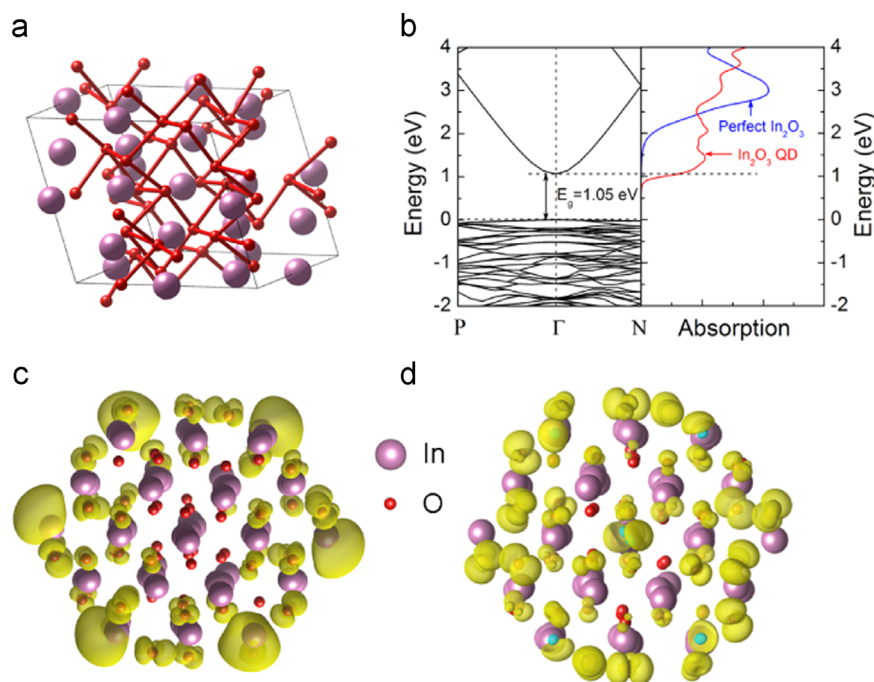
Fig. 4. Conceptual illustration of breaking the dipole-forbidden transition rule in an In_2O_3 quantum dot (QD). (a) Primitive cell of bixbyite In_2O_3. Red (small) and purple (large) balls represent oxygen and indium atoms, respectively. (b) Band structure of bulk In_2O_3 (left) and optical absorption spectra of bulk In_2O_3 and In_2O_3 QD (right) calculated using generalized gradient approximation. Partial charge densities of (c) lowest unoccupied molecular orbital and (d) highest occupied molecular orbital of an In_2O_3 QD with a diameter of 1.5 nm. (For interpretation of the references to color in this figure legend, the reader is referred to the web version of this article.)

are $4.0 \times 10^5 \; \Omega$ and 3.43, respectively, by fitting the $I–V$ data using the equation. The large series resistance is attributed to the high density structural defects which serve as the recombination centers and the physical contact between the two layers. The high turn-on voltage is attributed to the high series resistance. This can be caused by the physical contact between In_2O_3 and GaN, and the high-density structural defects which serve as the trap-assisted generation-recombination centers [37]. The inset of Fig. 3b shows the $I–V$ plots from the In-n-In_2O_3 contact. The linear trend indicated a good ohmic contact of indium electrodes on the n-In_2O_3 film, and implied that the rectifying behavior originates from the p–n junction instead of the Schottky contacts.

Fig. 3c shows the spectral response of the In_2O_3/p-GaN heterojunction photodiode under zero, forward and reverse bias of 5 V. There are two photoresponse peaks under zero bias condition: one peak of 1.6×10^{-4} A/W at 379 nm and another peak of 1.2×10^{-4} A/W at 338 nm. Compared with the optical bandgap of the In_2O_3 film and p-GaN substrate, the strong and weak response peaks are derived from the In_2O_3 layer and p-GaN substrate, respectively. When a forward bias of 5 V was applied, the photoresponse peaks became weaker. When a reverse bias of 5 V was applied, the peak at 379 nm significantly became strong, and the response peak reached up to 9.1×10^{-4} A/W. It is noted that the narrow response peak at 379 nm has a full width at half maximum of only 21 nm, suggesting that the responsivity of the photodiode is highly spectrum-selective. The inset in Fig. 3c shows the time-dependent photocurrent of the photodiode at the reverse bias of 5 V when a 380 nm light irradiates on the device with periodical turning on and off. The photocurrent increases to 3.0 μA and decreases to initial value, respectively, as the light was periodically turned on and off, suggesting the excellent reproducible characteristics.

We finally elucidate why the dipole-forbidden transition rule can be broken in the In_2O_3 nanocrystals using first-principles calculations. Fig. 4a and b shows the crystal structure of bulk bixbyite In_2O_3 primitive cell and the corresponding band

structure, respectively. The calculated fundamental bandgap of the bulk In_2O_3 is 1.05 eV. It should be pointed that GGA severely underestimates the bandgap of oxide materials. However, the wavefunction characters at the band edges cannot be significantly changed by the GGA calculation and the characters of the NBE optical transitions are not affected by the GGA bandgap error. Therefore, the underestimation of bandgap does not affect our discussion on the results. The calculated optical absorption spectra of the perfect In_2O_3 and In_2O_3 QD are shown in Fig. 4b. The onset of the optical absorption edge of the perfect In_2O_3 is much higher than the fundamental bandgap, indicating that the band-edge transition is not allowed. For the In_2O_3 QD, the onset of the optical absorption edge is at the fundamental gap, suggesting that the fundamental gap transition becomes allowed, namely, the optical transition between the highest occupied molecular orbital (HOMO) and the lowest unoccupied molecular orbital (LUMO) is allowed due to the surface states breaking the symmetry. Fig. 4c and d shows the partial charge densities of LUMO and HOMO of the In_2O_3 QD respectively. These charge densities are mainly distributed on the surface of the QD, indicating that breaking forbidden transition between LUMO and HOMO is derived from the surface defects, e.g. dangling bonds. Therefore, it is well understood why the band-edge emission/absorption is recovered in the In_2O_3 nanocrystals.

4. Conclusions

In summary, a hybrid In_2O_3 nanocrystals/amorphous film was deposited on quartz substrate by magnetron sputtering technique combining with post-annealing processing. The NBE UV emission and absorption were realized in the hybrid In_2O_3 film, suggesting that the nanocrystals/amorphous hybrid structure can alter the band symmetry and break the quantum mechanical dipole-forbidden transition rule. Using this approach, we also realized the In_2O_3-based photodiode with the highly spectrum-selective UV

responsivity in the NBE region. Our results suggest that tailoring In_2O_3 nanostructure is an effective route to achieving novel optical properties and applying these properties to the UV optoelectronic field.

Acknowledgments

References

[1] M. Jain, J.R. Chelikowsky, S.G. Louie, Quasiparticle excitations and charge transition levels of oxygen vacancies in hafnia, Phys. Rev. Lett. 107 (2011) 216803.

[2] A. Walsh, J.L.F. Da Silva, S.-H. Wei, C. Körber, A. Klein, L.F.J. Piper, A. DeMasi, K. E. Smith, G. Panaccione, P. Torelli, D.J. Payne, A. Bourlange, R.G. Egdell, Nature of the band gap of In_2O_3 revealed by first-principles calculations and X-ray spectroscopy, Phys. Rev. Lett. 100 (2008) 167402.

[3] D.C.La.J.W. Hemsky, Residual native shallow donor in ZnO, Phys. Rev. Lett. 82 (1999) 2552–2555.

[4] Y. Huang, Y. Li, B. Yao, Z. Ding, R. Deng, L. Zhang, H. Zhao, A facile route to realize ultraviolet emission in a nano-engineered SnO_2-based light-emitting diode, J. Phys. D: Appl. Phys. 48 (2015) 465103.

[5] W. Liu, B. Yao, Y. Li, B. Li, C. Zheng, B. Zhang, C. Shan, Z. Zhang, J. Zhang, D. Shen, Annealing temperature dependent electrical and optical properties of ZnO and MgZnO films in hydrogen ambient, Appl. Surf. Sci. 255 (2009) 6745–6749.

[6] Y. Li, W. Yin, R. Deng, R. Chen, J. Chen, Q. Yan, B. Yao, H. Sun, S.-H. Wei, T. Wu, Realizing a SnO_2-based ultraviolet light-emitting diode via breaking the dipole-forbidden rule, NPG Asia Mater. 4 (2012) e30.

[7] Y. Li, R. Deng, W. Lin, Y. Tian, H. Peng, J. Yi, B. Yao, T. Wu, Electrostatic tuning of Kondo effect in a rare-earth-doped wide-band-gap oxide, Phys. Rev. B 87 (2013) 155151.

[8] Y.F. Li, H.L. Pan, B. Yao, R. Deng, Y. Xu, J.C. Li, L.G. Zhang, H.F. Zhao, D.Z. Shen, T. Wu, Hole-mediated ferromagnetic enhancement and stability in Cu-doped ZnOS alloy thin films, J. Phys. D: Appl. Phys. 45 (2012) 075002.

[9] B. Zhang, B. Yao, S. Wang, Y. Li, C. Shan, J. Zhang, B. Li, Z. Zhang, D. Shen, Influence of Zn/O ratio on structural, electrical and optical properties of ZnO thin films fabricated by plasma-assisted molecular beam epitaxy, J. Alloy. Compd. 503 (2010) 155–158.

[10] Y. Li, R. Deng, B. Yao, G. Xing, D. Wang, T. Wu, Tuning ferromagnetism in $Mg_x Zn_{1-x}O$ thin films by band gap and defect engineering, Appl. Phys. Lett. 97 (2010) 102506.

[11] H.Y. Peng, Y.F. Li, W.N. Lin, Y.Z. Wang, X.Y. Gao, T. Wu, Deterministic conversion between memory and threshold resistive switching via tuning the strong electron correlation, Sci. Rep. 2 (2012) 442.

[12] B.Y. Zhang, B. Yao, Y.F. Li, Z.Z. Zhang, B.H. Li, C.X. Shan, D.X. Zhao, D.Z. Shen, Investigation on the formation mechanism of p-type Li–N dual-doped ZnO, Appl. Phys. Lett. 97 (2010) 222101.

[13] W.J. Maeng, D.-W. Choi, J. Park, J.-S. Park, Atomic layer deposition of highly conductive indium oxide using a liquid precursor and water oxidant, Ceram. Int. 41 (2015) 10782–10787.

[14] A. Dixit, R.P. Panguluri, C. Sudakar, P. Kharel, P. Thapa, I. Avrutsky, R. Naik, G. Lawes, B. Nadgorny, Robust room temperature persistent photoconductivity in polycrystalline indium oxide films, Appl. Phys. Lett. 94 (2009) 252105.

[15] H.-M. Lee, S.-B. Kang, K.-B. Chung, H.-K. Kim, Transparent and flexible amorphous In–Si–O films for flexible organic solar cells, Appl. Phys. Lett. 102 (2013) 021914.

[16] J.-H. Lim, D.-K. Hwang, H.-S. Kim, J.-Y. Oh, J.-H. Yang, R. Navamathavan, S.-J. Park, Low-resistivity and transparent indium-oxide-doped ZnO ohmic contact to p-type GaN, Appl. Phys. Lett. 85 (2004) 6191.

[17] H.Y. Yang, S.F. Yu, H.K. Liang, T.P. Chen, J. Gao, T. Wu, Electroluminescence from In_2O_3:Sn randomly assembled nanorods/p-SiC heterojunction, Opt. Express 18 (2010) 15585–15590.

[18] J. Gao, O.I. Lebedev, S. Turner, Y.F. Li, Y.H. Lu, Y.P. Feng, P. Boullay, W. Prellier, G. van Tendeloo, T. Wu, Phase selection enabled formation of abrupt axial heterojunctions in branched oxide nanowires, Nano Lett. 12 (2011) 275–280.

[19] X. Liang, G. Jin, F. Liu, X. Zhang, S. An, J. Ma, G. Lu, Synthesis of In_2O_3 hollow nanofibers and their application in highly sensitive detection of acetone, Ceram. Int. 41 (2015) 13780–13787.

[20] G. Korotcenkov, I. Boris, V. Brinzari, S.H. Han, B.K. Cho, Y.N. Lychkovsky, In_2O_3:Ga and In_2O_3:P-based one-electrode gas sensors: comparative study, Ceram. Int. 41 (2015) 7478–7488.

[21] Q. Liu, W. Zhang, R. Liu, G. Mao, Controlled synthesis of monodispersed sub-50 nm nanoporous In_2O_3 spheres and their photoelectrochemical performance, Eur. J. Inorg. Chem. 2015 (2015) 845–851.

[22] Y. Ohhata, F. Shinoki, S. Yoshida, Optical properties of rf reactive sputtered tin-doped In_2O_3 films, Thin Solid Films 59 (1979) 255–261.

[23] I. Hamberg, C.G. Granqvist, K.F. Berggren, B.E. Sernelius, L. Engström, Band-gap widening in heavily Sn-doped In_2O_3, Phys. Rev. B 30 (1984) 3240–3249.

[24] V.T. Agekyan, Spectroscopic properties of semiconductor crystals with direct forbidden energy gap, Phys. Status Solidia 43 (1977) 11–42.

[25] Z.P. Wei, D.L. Guo, B. Liu, R. Chen, L.M. Wong, W.F. Yang, S.J. Wang, H.D. Sun, T. Wu, Ultraviolet light emission and excitonic fine structures in ultrathin single-crystalline indium oxide nanowires, Appl. Phys. Lett. 96 (2010) 031902.

[26] H. Zhou, W. Cai, L. Zhang, Photoluminescence of indium-oxide nanoparticles dispersed within pores of mesoporous silica, Appl. Phys. Lett. 75 (1999) 495.

[27] D. Yu, S.H. Yu, S. Zhang, J. Zuo, D. Wang, Y.T. Qian, Metastable hexagonal In_2O_3 nanofibers templated from InOOH nanofibers under ambient pressure, Adv. Funct. Mater. 13 (2003) 497–501.

[28] M. Shi, F. Xu, K. Yu, Z. Zhu, J. Fang, Controllable synthesis of In_2O_3 nanocubes, truncated nanocubes, and symmetric multipods, J. Phys. Chem. C 111 (2007) 16267–16271.

[29] G. Kresse, J. Furthmüller, Efficient iterative schemes for ab initio total-energy calculations using a plane-wave basis set, Phys. Rev. B 54 (1996) 11169–11186.

[30] P.E. Blöchl, Projector augmented-wave method, Phys. Rev. B 50 (1994) 17953–17979.

[31] R.L. Weiher, Optical properties of indium oxide, J. Appl. Phys. 37 (1966) 299.

[32] M. Gholampour, A. Abdollah-zadeh, L. Shekari, R. Poursalehi, A catalyst free method to grow GaN nanowires on porous Si at low temperature, Ceram. Int. 41 (2015) 13855–13860.

[33] H. Lu, X. Meng, Correlation between band gap, dielectric constant, Young's modulus and melting temperature of GaN nanocrystals and their size and shape dependences, Sci. Rep. 5 (2015) 16939.

[34] F.P. Sabino, R. Besse, L.N. Oliveira, S.-H. Wei, J.L.F. Da Silva, Origin of and tuning the optical and fundamental band gaps in transparent conducting oxides: the case of M_2O_3 (M = Al,Ga,In), Phys. Rev. B 92 (2015) 205308.

[35] N. Tripathi, S. Rath, Effect of thermal annealing and swift heavy ion irradiation on the optical properties of indium oxide thin films, ECS J. Solid State Sci. Technol. 3 (2013) P21–P25.

[36] C.J. Chen, W.L. Xu, M.Y. Chern, Low-temperature epitaxial growth of vertical In_2O_3 nanowires on A-plane sapphire with hexagonal cross-section, Adv. Mater. 19 (2007) 3012–3015.

[37] T.T. Anh Tuan, D.-H. Kuo, Temperature-dependent electrical properties of the sputtering-made n-InGaN/p-GaN junction diode with a breakdown voltage above 20 V, Mater. Sci. Semicond. Process. 32 (2015) 160–165.